2013

Keratin gene expression profiles after digit amputation in C57BL/6 vs. regenerative MRL mice imply an early regenerative keratinocyte activated-like state

Chia-ho Cheng

John Leferovich

Xiangming Zhang

Khamilia Bedelbaeva

Dmitri Gourevitch

See next page for additional authors

Keratin gene expression profiles after digit amputation in C57BL/6 vs. regenerative MRL mice imply an early regenerative keratinocyte activated-like state

Chia-Ho Cheng, John Leferovich, Xiang-Ming Zhang, Khamilia Bedelbaeva, Dmitri Gourevitch, Cathy J. Hatcher, Craig T. Basson, Ellen Heber-Katz and Kenneth A. Marx

Physiol. Genomics 45:409-421, 2013. First published 19 March 2013;
doi:10.1152/physiolgenomics.00142.2012

Physiol Genomics 45: 409–421, 2013.
First published March 19, 2013; doi:10.1152/physiolgenomics.00142.2012.

Keratin gene expression profiles after digit amputation in C57BL/6 vs. regenerative MRL mice imply an early regenerative keratinocyte activated-like state

Chia-Ho Cheng,[1] John Leferovich,[2] Xiang-Ming Zhang,[2] Khamilia Bedelbaeva,[2] Dmitri Gourevitch,[2] Cathy J. Hatcher,[3] Craig T. Basson,[4] Ellen Heber-Katz,[2] and Kenneth A. Marx[1]

[1]*Center for Intelligent Biomaterials, Department of Chemistry, University of Massachusetts Lowell, Lowell, Massachusetts;* [2]*The Wistar Institute, Philadelphia, Pennsylvania;* [3]*Center for Molecular Cardiology, Greenberg Division of Cardiology, Weill Cornell Medical College, New York, New York; and* [4]*Novartis Institutes for Biomedical Research, Cambridge, Massachusetts*

Submitted 25 October 2012; accepted in final form 18 March 2013

Cheng CH, Leferovich J, Zhang XM, Bedelbaeva K, Gourevitch D, Hatcher CJ, Basson CT, Heber-Katz E, Marx KA. Keratin gene expression profiles after digit amputation in C57BL/6 vs. regenerative MRL mice imply an early regenerative keratinocyte activated-like state. *Physiol Genomics* 45: 409–421, 2013. First published March 19, 2013; doi:10.1152/physiolgenomics.00142.2012.—Mouse strains C57BL/6 (B6) and MRL were studied by whole mouse genome chip microarray analyses of RNA isolated from amputation sites at different times pre- and postamputation at the midsecond phalange of the middle digit. Many keratin genes were highly differentially expressed. All keratin genes were placed into three temporal response classes determined by injury/preinjury ratios. One class, containing only *Krt6* and *Krt16,* were uniquely expressed relative to the other two classes and exhibited different temporal responses in MRL vs. B6. Immunohistochemical staining for Krt6 and Krt16 in tissue sections, including normal digit, flank skin, and small intestine, and from normal and injured ear pinna tissue exhibited staining differences in B6 (low) and MRL (high) that were consistent with the microarray results. Krt10 staining showed no injury-induced differences, consistent with microarray expression. We analyzed *Krt6 and Krt16* gene association networks and observed in uninjured tissue several genes with higher expression levels in MRL, but not B6, that were associated with the keratinocyte activated state: *Krt6*, *Krt16*, *S100a8*, *S100a9,* and *Il1b*; these data suggest that keratinocytes in the MRL strain, but not in B6, are in an activated state prior to wounding. These expression levels decreased in MRL at all times postwounding but rose in the B6, peaking at *day 3*. Other keratins significantly expressed in the normal basal keratinocyte state showed no significant strain differences. These data suggest that normal MRL skin is in a keratinocyte activated state, which may provide it with superior responses to wounding.

keratin genes; microarrays; MRL mouse; digit amputation; keratinocyte activation cycle

THE ABILITY TO REGENERATE amputated appendages is generally associated only with amphibians (6, 33). It is not a characteristic associated with mammals though there are several exceptions. The closure of ear holes with the formation of a blastema and the regrowth of cartilage have been reported in the rabbit (18) and in a single mouse strain, the MRL (10), and its parent strain LG/J (27). The digit tip has been shown to regrow in both mouse and human (4, 7, 21, 25, 31, 32, 43, 47), though amputation below the first proximal joint leads to scarring and no growth (25, 31). Studies of digit amputation in the second phalange in the MRL mouse has indicated that blastema formation does occur but is followed after 2 wk by an apoptotic response eliminating new tissue. This is followed by a second attempt at blastema formation. However, full regrowth and replacement of lost tissue are not seen. This is in contrast to the response seen in C57BL/6 (B6) and Swiss Webster (SW) mouse tissue in which blastema formation is never seen (20).

In the current study, we explored the genes involved in a digit amputation response model in both MRL and B6 mice. Tissue was obtained on *days 0, 3, 7,* and *14* postdigit amputation and analyzed by microarray analysis. Two related gene families in particular stood out as differing significantly in their expression patterns between MRL and B6, the *Krt* and *Krtap* gene families. Upon examination of direct gene expression levels in each strain and ratios of injured vs. normal tissue, we observed three different patterns of expression with the following properties. In *class 1*, containing only two genes, the *Krt* genes *Krt6* and *Krt16* were initially expressed at low levels in uninjured B6 and then upregulated following injury and were initially expressed at high levels in uninjured MRL but then were downregulated following injury. In *class 2*, *Krt* genes were initially expressed at high levels in uninjured B6 tissue but then were downregulated following injury, while in uninjured MRL they were expressed at low levels followed by higher levels following injury. In *class 3*, *Krt* genes exhibited no significant expression differences over time. Examination of the *Krt6* and *Krt16* genes at the level of protein expression showed differences not only in the digit but also in regenerating MRL and B6 ear tissue, flank skin, and small intestine.

Epidermal keratinocytes exhibit two alternative pathways: differentiation and activation. The activation pathway is launched in response to epidermal injury or certain pathologic conditions (17). Given that *Krt6 and Krt16* are considered to be markers of keratinocyte activation (17), our data suggest that the keratinocyte in MRL mouse skin is in an activated state. Further exploration of expression data for other genes supported the existence of this activated state in the MRL prior to wounding.

METHODS

Mice. Female mice, ages 3–4 mo, were used in all experiments. The MRL/MpJ (MRL) mice were obtained from the Jackson Laboratories (Bar Harbor, ME), and the B6 mice were obtained from

Address for reprint requests and other correspondence: K. A. Marx, Center for Intelligent Biomaterials, Dept. of Chemistry, Univ. of Massachusetts Lowell, Lowell, MA 01854 (e-mail: kenneth_marx@uml.edu).

Taconic Laboratories (Germantown, NY). Animals were maintained under standard conditions at the Wistar Institute Animal Facility (Philadelphia, PA), and the protocols were in accordance with institutional regulations.

Surgical procedures. Mice were anesthetized with ketamine-xylazine (90/9 mg/kg ip). Both hind feet were scrubbed with chlorohexaderm and rinsed with 70% ethanol. Using a #10 scalpel, we amputated the middle digit on both rear paws at the level of 50% of the second phalanx. Bleeding was controlled by digital pressure and sterile gauze. Subsequent to amputation, animals were given buprenorphine (2 mg/kg sc) every 6–8 h for 2 days for analgesia. Animals were observed during anesthetic recovery to ensure hemostasis. Mice were euthanized at various times postsurgery with CO_2 to obtain RNA and histological specimens. This surgery protocol was approved by the Wistar Institute Institutional Animal Care and Use Committee.

Histological techniques. Digit tissue was treated with Carnoy's fixative for 24 h, followed by decalcification with Morse's decalcifying solution for 24–48 h as previously described (20), subjected to final processing with a Citadel 1000 Shandon Tissue Processor (Thermo-Fisher), and then paraffin embedded. Later, 5 μm thick sections were cut. Samples were collected from at least three separate animals for each time point and strain. Ear tissue was treated with Prefer fixative, followed by ETOH, and then PBS each for 24 h. Paraffin embedding was followed by sectioning of tissues at 5 μm.

Immunohistochemistry. To examine keratin expression, immunostaining with antibodies for Krt6 (Neomarkers cat. #MS-766-PO, mouse monoclonal, 1:100 dilution), Krt10 (Chemicon cat. #MAB1605; mouse monoclonal, 1:100 dilution); and Krt16 (Epitomics cat. #2142-1, rabbit monoclonal, 1:100) was performed. Tissue sections were incubated with 2% BSA as a blocking buffer for 1 h, at room temperature (RT), then primary antibody was applied for 16 h at +4°C. After washing the tissue in 1× PBS, we applied secondary antibody for 1 h RT. Alexa Fluor 594-labeled goat anti-mouse secondary antibody (1:500; Molecular Probes, Invitrogen, cat. #A11005) was used for detecting Krt6 and Krt10 and Alexa Fluor 488 goat anti-mouse secondary antibody (1:500, cat. #A11008; Molecular Probes, Invitrogen) was used for detecting Krt16. Controls were carried out with secondary antibodies alone after BSA blocking of tissue. For quantitation and image analysis, ImageJ v1.46f software, provided by the National Institutes of Health (NIH), was used. The entire area of newly formed tissue plus an additional tissue zone of 100–150 μm of the surrounding distal aspect of the cartilage was analyzed.

RNA analyses. Total RNA was isolated from injured and normal digits by homogenizing individual digits in TRIzol (Gibco) with further processing and purification using an RNeasy Mini kit (Qiagen cat. #74104). Three replicates from each strain for each time point was analyzed, and two digits from MRL and four to six digits from B6 were used for each replicate. Amputation was performed as shown in Fig. 1 where the digit tip was excluded and included tissue only from the second phalange. The Genomics Resources Core Facility at Weill Cornell Medical College performed the preparation of cRNA, quality control, and hybridized microarray chips. Briefly, the quantity and quality of the total RNA were assessed using the NanoDrop ND-1000 Spectrophotometer (Thermo Scientific, Wilmington, DE) and Agilent Bioanalyzer (Santa Clara, CA). For the microarray analyses we enriched for mRNA species from 1 μg of total RNA by reduction of the 28S and 18S rRNA species with the RiboMinus Human/Mouse Transcriptome isolation Kit (Invitrogen) according to the manufacturer's protocol. Reduction of rRNA minimizes background and thereby increases array detection sensitivity and specificity. Double-stranded cDNA was synthesized and transcribed into sense cRNA that was reverse transcribed into single-stranded (ss) sense DNA. The ssDNA was fragmented and subsequently biotinylated through labeling with recombinant terminal deoxynucleotidyl transferase covalently linked to biotin with the Whole Transcript Sense Target Labeling Kit (Affymetrix) according to the manufacturer's protocol. The biotinylated cDNA was hybridized to the GeneChip Mouse Exon 1.0 ST arrays (Affymetrix) for analysis of >80,000 transcripts present on a single array. Following array hybridization, the GeneChip arrays were washed, stained, and scanned by GeneChip Scanner 3000 7G according the manufacturer's instructions (Affymetrix Expression Analysis technical manual). Affymetrix GeneChip Command Console Software was used for image acquisition to provide data for "gene level" expression analysis only. All microarray analyses were performed in triplicate. Three separate chip experiments were performed for each normal tissue and each day postamputation for both B6 and MRL strains. For quantitative reverse transcriptase-PCR (q-rtPCR), 1 μg of total RNA was reverse transcribed into cDNA (iScript cDNA synthesis kit, Bio-Rad) that served as a template for real-time PCR analysis of mRNA expression (LightCycler 480 SYBR Green I Master kit, Roche). PCR reactions were performed on a Roche LightCycler under the following conditions: 95°C for 5 min, followed by 95°C for 10 s, 58°C for 20 s, and 72°C for 30 s for 45 cycles. Primer sequences used to amplify the mouse transcripts, including *Krt6a*, *Krt6b*, *Krt10*, *Krt16,* and *GAPDH*, were designed to span exon-exon boundaries (Table 1) Primer pairs were initially tested in standard PCR and shown to amplify a single product by agarose gel electrophoresis prior to q-rtPCR. Linearity of the threshold values (C_T) was confirmed by running a dilution series of cDNA with each primer pair. Changes in gene expression were determined by averaging C_T values for duplicate PCR reactions from three mouse digits and calculated as % change compared with control samples and expressed in values normalized to *GAPDH* mRNA expression as previously described (22). All gene expression values are expressed as means ± SE from

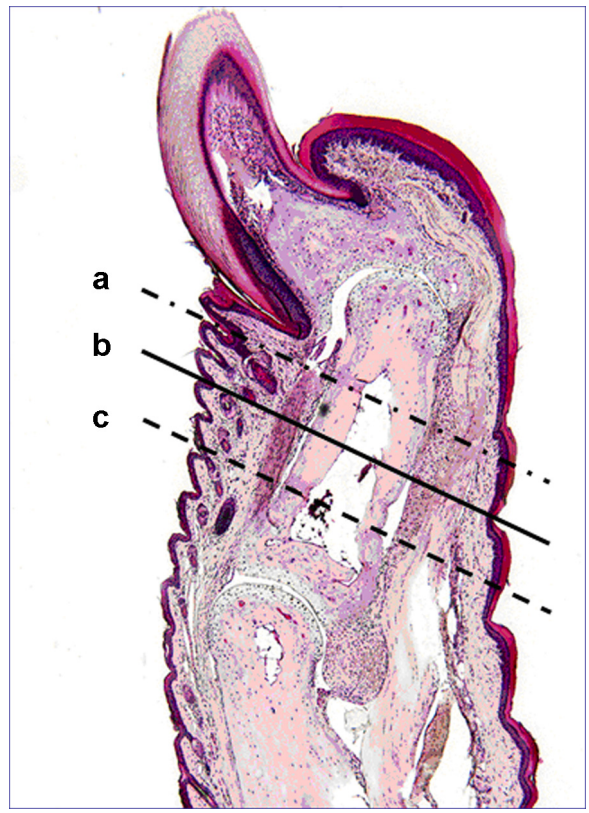

Fig. 1. The longitudinal hematoxylin and eosin H&E section of an uninjured MRL digit. The area between the broken lines (a, c) indicates the uninjured tissue (*day 0*) that was analyzed. The solid line (b) indicates the level at which each digit was subjected to amputation injury. The area analyzed as injured tissue included tissue from *line c* through *line b* and any new tissue that resulting from healing.

Table 1. *Primer sequences for quantitative reverse transcriptase PCR*

Gene	Primer Sequence	Product Size, bp
Krt6a	Forward: 5′ATCCCGTGCTCAGAGCCCCGAGT−3′	402
	Reverse: 5′CACAGGACCAGTGACGGGGCAG-3′	
Krt6b	Forward: 5′AGTGCCCTGTGTACGGGGTCGTG−3′	214
	Reverse: 5′ACAGAGGTAGGGAGGGAGGAGCCT-3′	
Krt10	Forward: 5′CGGTGGAGGTGGCAGCTTCGG−3′	247
	Reverse: 5′CTCGCTGGCTTGAGTTGCCATGCTT−3′	
Krt16	Forward: 5′ATGACCGCCTGGCCACCTACCTGGAC−3′	280
	Reverse: 5′CCCTCCACGGACTGCCGCAAGAA−3′	
GAPDH	Forward: 5′ATTCAACGGCACAGTCAAGG−3′	467
	Reverse: 5′TGGATGCAGGGATGATGTTC−3′	

the triplicate experiments. Statistical analyses were performed by ANOVA or Student's *t*-test. $P < 0.05$ was considered significant.

Microarray data processing and statistical analysis. The robust multiarray average in Expression Console software (Affymetrix, Santa Clara, CA) was used for background correction, normalization, and probe set summarization as gene-level analysis, rather than exon level analysis (5, 37). In the following filtering step, the significance analysis microarray (SAM) algorithm (42) was used with a false discovery rate of <5% to process each of the normalized datasets for individual genes' statistical significance between the ratios *day X* and *day 0*, where X = 3, 7, and 14 for both MRL and B6. A total of 12,772 genes passed SAM analysis at least for one of six conditions. With the further criteria of more than twofold change, six different day-specific gene subsets for MRL *day 3* (430 genes), *day 7* (310 genes), *day 14* (391 genes), and B6 *day 3* (1,016 genes), *day 7* (965 genes), and *day 14* (660 genes) were generated that met the significance criteria. Other statistical analyses for *t*-test and Fisher's exact test in this document were implemented in the R language. The complete raw and normalized microarray data have been deposited in National Center for Biotechnology Information's Gene Expression Omnibus (GEO) and are accessible through GEO Series accession number GSE26227 (http://www.ncbi.nlm.nih.gov/geo/query/acc.cgi?acc=GSE26227). The microarray analyses we performed are presented in Figs. 2–9 and Table 2 in this study.

Pathways analysis. STRING (http://string.embl.de/), a web-based protein interactions database (26), was used to create the mouse first nearest neighbors based protein-protein interaction (PPI) network shown in Fig. 8. The PPI network was created starting with Krt16 and Krt6b and a number of other prominent proteins (*Csf1*, Csf2, Csf3, Egf, Egfr, Icam1, Ifng, Il1a, Il1b, Il1rn, Il3, Il6, Il8rb, krt1, krt10, krt14,Krt17, Krt5, Tgfa, Tgfb1, Tgfb2, Tgfb3, Tnf, Tnfaip3, S100a8, and S100a9), defining the keratinocyte activation cycle as described in a review article (17). The result was a network with 40 genes and 313 interactions with the medium confidence score level defined by STRING. Cytoscape (http://www.cytoscape.org/), an open-source software for pathway analysis (11), was subsequently used to create the visual representation of the PPI network applying our microarray results of individual gene strain expression differences between B6 and MRL mice based on the build network from STRING (see Fig. 8).

RESULTS

Total genome and keratin gene expression response. Microarray experiments were carried out with RNA extracted from digit amputation tissue as depicted in Fig. 1. Out of 16,661 genes represented on the Affymetrix mouse exon 1.0 array mouse genome chip, 12,772 genes passed the SAM statistical test. These genes' expression behavior was initially examined as lists of upregulated or downregulated genes ranked by fold-change (data not shown). There appeared to be a significant enrichment in keratin genes and keratin-associated genes in these lists that possessed high fold-change levels postamputation. For this reason we compare in Fig. 2 the temporal behavior of *Krt* and *Krtap* genes to all expressed genes on the chip. The data point for every gene is displayed as a $\log_2$(ratio) for each day postamputation normalized to *day 0* for the MRL strain values (*y*-axis) plotted vs. the B6 strain values (*x*-axis). *Krts* and *Krtaps* are presented as filled symbols, while all other genes are open symbols. Figure 2, *A, B,* and *C,* displays the respective fold-change expression levels for *day 3* compared with *day 0*, *day 7* with *day 0*, and *day 14* with *day 0*. In Fig. 2*A*, there is a clear total gene expression trend for *day 3* compared with *day 0*, in that the subset of genes most upregulated in the B6 strain tended to be most downregulated in the MRL strain. By contrast, the subset of genes most downregulated in B6 were most upregulated in MRL. There is no similar trend evident in Fig. 2*B day 7* compared with *day 0* or in Fig. 2*C day 14* compared with *day 0*, The large fold-change response genes displayed a significant enrichment in both keratins (*Krts*) or keratin-associated proteins (*Krtaps*), with most showing B6 downregulation and MRL upregulation on going from *day 0* to *day 3*. Figure 2, *B* and *C*, displays a somewhat similar behavior for *Krt* and *Krtap* genes.

Apart from the visual fold-change enrichment of *Krt* and *Krtap* genes observed in Fig. 2, we wished to assess the statistical significance of their enrichment. To carry this out numerically we established arbitrary binning criteria of twofold upregulation or downregulation. For each category, the numbers of total genes and *Krt* and *Krtap* genes were determined that were, respectively, more than twofold upregulated or more than twofold downregulated relative to their uninjured control tissue levels (data not shown). Next, we examined the % of *Krt* and *Krtap* genes contained within the more than twofold upregulated and downregulated gene groups for each mouse strain at each time point as well as the % ratio for the MRL relative to the B6 strain. Within the group of genes upregulated more than twofold, the MRL strain contains a significant number that are *Krt* and *Krtap* genes, while the B6 strain contains very few, clearly indicating MRL is enriched in upregulated *Krt* and *Krtap* genes. Determining the *% Krt* and *% Krtap* genes in the total over twofold upregulated genes, there is 37-fold more *Krt* and *Krtap* genes upregulated in MRL than those in B6 at *day 3* postamputation. Just the opposite fold-change behavior is exhibited within the more than twofold downregulated genes. For this criterion, the *% Krt* and *% Krtap* genes in MRL varies from 0.08 to 0.24 that of B6 for *days 3–14* postamputation. Statistical analysis of these enrichment data by Fisher's exact test, where our sample sizes are small, demonstrated a statistically significant difference (all have *P* value < 0.02, data not shown) in the % of *Krt* and *Krtap* genes upregulated or downregulated between the B6 and MRL strains for all postamputation time points with the exception of the twofold upregulated genes on *day 7*. Therefore, in our study we focused on characterizing this statistically significant *Krt* and *Krtap* gene differential temporal expression behavior in the two mouse strains.

Chromosome 11 locus and individual krt and krtap gene behavior. In the mouse genome, *Krt* and *Krtap* gene loci are located on chromosomes (chr) 7, 11, 15, and 16. The majority of *Krt* genes reside on chr 11 and 15. The few genes on chr 7 exhibited unremarkable expression change behavior (data not

Table 2. Krt *and* Krtap *gene identities, chromosomal locations, and expression behaviors in B6 vs. MRL strains*

Gene Symbol	Chr	Class	B6_D0	MRL_D0	B6_D3/B6_D0	MRL_D3/MRL_D0
Krtap5-4	7		4852	855	0.04	4.99
Krtap5-2	7		2288	423	0.06	4.45
Krt16	11	1	443 [88889]	3610 [356524]	11.96 [2.5]	0.40 [0.6]
Krt25	11	2	5543	1158	0.10	4.27
Krt27	11	2	5483	1069	0.09	4.37
Krt15	11	2	4519	2297	0.40	1.91
Krtap3-3	11	2	4331	1021	0.07	4.89
Krtap17-1 ///Krt33a	11	2	2835	504	0.05	6.80
Krt35	11	2	1835	232	0.06	6.74
Krt31	11	2	1562	183	0.05	6.14
Krtap4-7	11	2	1335	244	0.03	4.08
Krt32	11	2	1096	150	0.06	6.94
Krt34	11	2	758	161	0.08	4.26
Krtap3-2	11	2	612	198	0.10	2.93
Krt23	11	2	513	250	0.40	2.13
Krt39	11	2	512	127	0.14	4.97
Krt19	11	2	116	80	0.53	1.64
Krt10	11	3	11413 [9205110]	11648 [1683930]	0.92 [0.04]	1.06 [1.26]
Krt14	11	3	9056	9461	1.13	0.95
Krt17	11	3	5583	5243	0.75	1.10
Krt42	11	3	130	116	0.87	1.07
Krt12	11	3	117	104	0.87	1.05
Krt222	11	3	39	33	0.78	0.98
Krt6a	15	1	816 [95887]	2082 [192461]	3.38 [1.48]	0.42 [0.76]
Krt6b	15	1	134 [39609]	6151 [1650825]	56.66 [26.65]	0.16 [1.18]
Krt71	15	2	7861	2025	0.11	3.79
Krt73	15	2	2868	612	0.08	4.99
Krt75	15	2	1465	377	0.16	3.58
Krt82	15	2	1236	237	0.08	5.04
Krt81 /// 5430421N21Rik /// Krt83	15	2	972	174	0.09	5.05
Krt72	15	2	869	193	0.10	4.49
Krt74	15	2	126	48	0.26	2.49
Krt2	15	3	11398	10206	0.56	1.19
Krt1	15	3	9162	10306	1.03	0.97
Krt79	15	3	4876	3040	0.52	1.48
Krt78	15	3	511	603	0.82	1.34
Krt84	15	3	297	616	0.48	1.62
Krt77	15	3	146	95	0.62	1.31
Krt7 /// Krt86	15	3	114	93	0.81	1.07
Krt18	15	3	107	77	0.58	1.20
Krt4	15	3	76	61	0.77	1.02
Krtap16-8	16		3629	245	0.07	1.45
Krtap16-8	16		2866	801	0.10	2.88
Krtap13-1	16		2492	384	0.07	5.53
Krtap26-1	16		1883	250	0.07	6.64
Krtap6-1 /// Krtap16-8	16		1746	236	0.06	3.06
Krtap16-8	16		1692	237	0.09	3.10
Krtap6-2	16		1564	150	0.06	3.82
Krtap14	16		1468	203	0.09	5.66
Krtap8-2	16		1076	238	0.08	3.58
Krtap16-5	16		836	86	0.11	4.02
Krtap16-4	16		615	109	0.13	2.41
Krtap16-1	16		433	76	0.09	5.04
Krtap16-3 /// Krtap16-6 /// Krtap16-10	16		243	24	0.06	2.80
Krtap13	16		11	53	1.32	1.27

Bracketed numbers represent gene expression levels determined by q-rtPCR.

shown); thus, we focused our analyses on chr 11 and 15 *Krt* and *Krtap* genes.

We examined the temporal response of individual *Krt* and *Krtap* genes following digit amputation. In Fig. 3, the *Krt* and *Krtap* chr 11 locus gene expression ratios are presented for B6 in Fig. 3*A* and for MRL in Fig. 3*B*. The *x*-axis displays the postamputation time points assayed with expression ratios presented as $\log_2$ (*day X/day 0*) values. Each temporal response line in Fig. 3 represents the behavior of a single gene over time. Some genes exhibit dramatically different behavior between B6 and MRL mice, while others show minor to negligible differences. The *Krt* and *Krtap* responses can be divided into three classes of response ratios: *1*) high in B6 but low in MRL, which contains just one gene, *Krt16*; *2*) low in B6 but high in MRL; and *3*) largely unchanged in B6 and MRL. Based on the *t*-test for significance, *class 2* vs. *3* show significant differences in their means ($P < 6.8E\text{-}12$), while the *class 1* mean (3.58) falls at least 6 standard deviations (0.58) beyond the mean of *class 2* (-0.54). This demonstrates that these three response ratio classes are statistically distinct from each other. *Krt16*

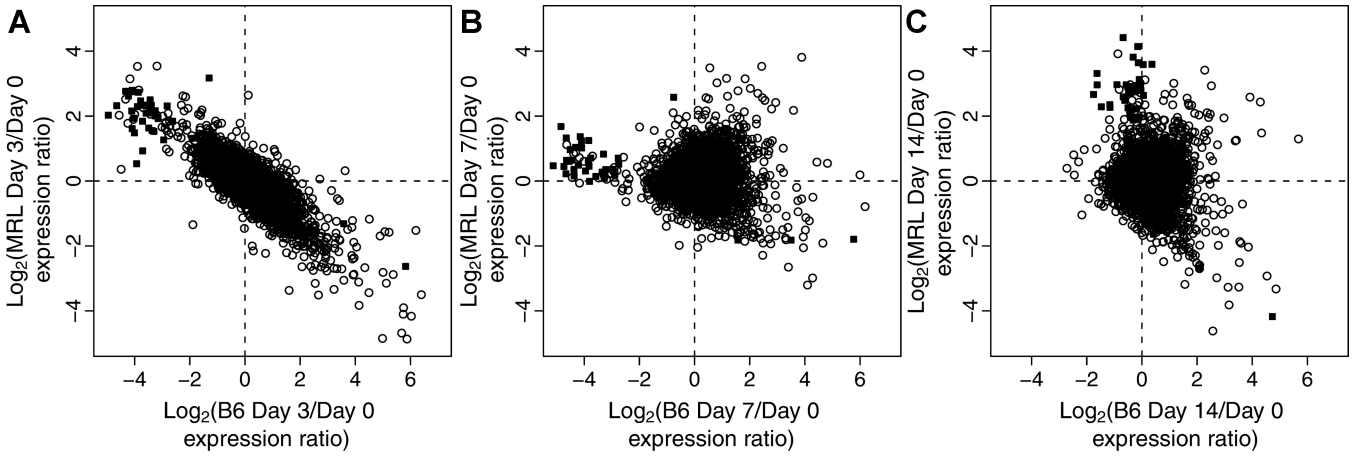

Fig. 2. Temporal $\log_2$(expression fold-change) from microarray data of digit amputation RNAs where the MRL vs. B6 values for each gene are plotted. *A*: *day 3/day 0* fold-change, *B*: *day 7/day 0* fold-change, *C*: *day 14/day 0* fold-change. In all panels, all genes on the chip are presented as open circles (○), while the *Krts* and *Krtaps* genes are presented as filled squares (■).

exhibits unique behavior and is the only *Krt* or *Krtap* chr 11 gene showing upregulation in B6 but downregulation in MRL after *day 0*.

In Table 2 we provide a summary of all the *Krt* and *Krtap* genes' chromosomal location, identity, class type, and initial expression behaviors. For both chr 7 and 16 the genes behave similarly to the *class 2* genes we observed on chromosomes 11 and 15. In the case of the chromosome 11 and 15 genes, Table 2 also contains the data for the large assembly of *Krtap* proteins that exist on chr 16. These keratin-associated protein species all possess similar characteristics to the keratin *class 2* proteins. They are all highly expressed in B6, but low in MRL at *day 0*, and then subsequently reverse their gene expression levels significantly by *day 3*.

Next, we examined the absolute expression levels of individual *Krt* and *Krtap* genes between the B6 and MRL strains to provide insights into differences between nonregnerating B6 vs. regenerating MRL mouse strain behavior not provided by an expression ratio change view. Figure 4, *A* and *B*, displays absolute gene expression levels ($\log_{10}$ values) for the same

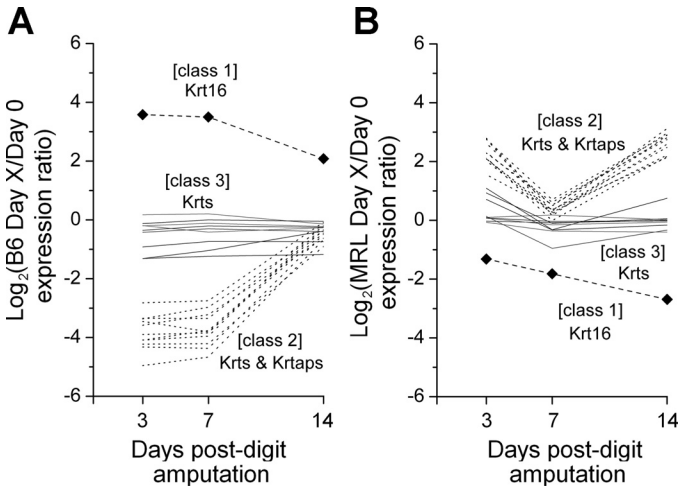

Fig. 3. Temporal $\log_2$(expression fold-change) from microarray data of digit amputation RNAs for *Krts* and *Krtaps* located on Chromosome 11 are displayed for B6 in *A* and for MRL in *B*. The 3 gene expression classes represented are described in the text. Each line represents the activity of a single gene in B6 (*day 0* normalized values at *days 3, 7, 14*; *A*) and in MRL (*day 0* normalized values at *days 3, 7, 14*; *B*) mice with *Krt16* (diamonds) specifically represented. The 3 expression classes are indicated with different line styles to code the individual lines.

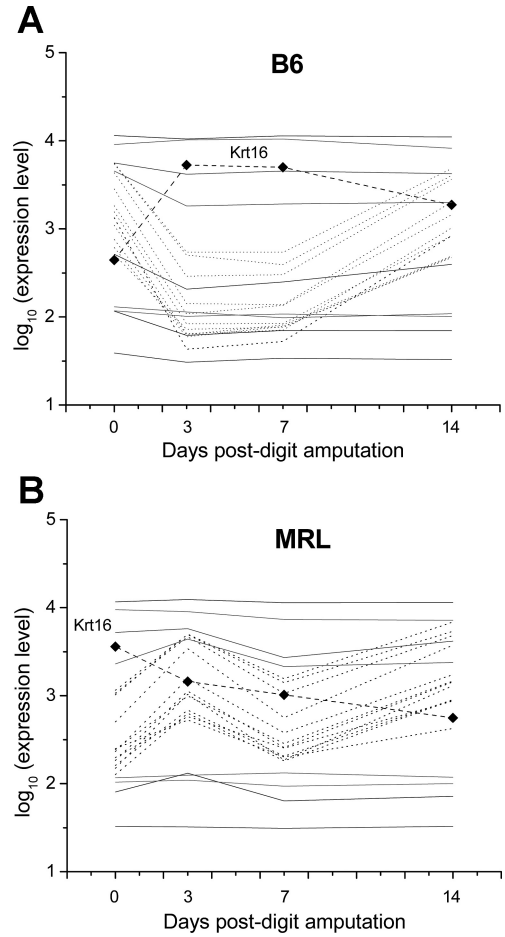

Fig. 4. Absolute temporal $\log_{10}$(expression Levels) of digit amputation RNAs for *Krts* and *Krtaps* on Chromosome 11 in B6 (*A*) and in MRL (*B*). The 3 gene expression classes represented are described in the text. The 3 expression classes with line styles identified in Fig. 3 are used to code the individual lines in these plots.

genes presented as expression ratios in Fig. 3, *A* and *B*. Here, the same three expression pattern classes are represented. *Class 3* genes, with unchanged expression ratio levels, possess values that cover ~320-fold expression level difference in both B6 and MRL strains. *Class 2* genes, with expression ratios low in B6 and high in MRL, cover a lower range of absolute expression levels, ~10-fold in both B6 and MRL strains. An obvious strain difference exists between *day 0* uninjured tissues and the earliest *day 3* postamputation tissue values. B6 and MRL strains start with very different expression levels of each of the *class 2* genes with B6 genes more highly expressed at *day 0* but dropping significantly by *day 3*. By contrast, MRL exhibits the exact opposite behavior; the same genes start at lower expression levels than B6 but rise significantly from *day 0* to *day 3* postamputation. In both strains, these genes are expressed at near similar levels at *days 7* and *14*. The single *class 1* gene, *Krt16*, exhibited a response (Fig. 4) that is opposite to that of the *class 2* genes. In uninjured tissue at *day 0*, absolute expression was low in the B6 strain but was significantly higher in MRL. By *day 3*, the expression levels had increased ~12-fold in B6 but decreased in MRL to ~40% of their initial values.

Our microarray analysis of *Krt* gene expression was confirmed by q-rtPCR analysis of *Krt10* and *Krt16* mRNA expression in the regenerating mouse digits, as shown in Table 2. The *class 1* gene, *Krt16*, and the *class 3* gene, *Krt10,* displayed similar absolute mRNA expression levels at *day 0*. *Krt16* and *Krt10* exhibited changes in *day 3* postamputation mRNA expression that mirrored our microarray data in B6 and MRL mice.

Chr15 locus and individual krt gene behavior. Chr 15 *Krt* gene expression ratios (Fig. 5) behave similarly to the chr 11 *Krt* and *Krtap* genes in Fig. 3 and can be divided into the same three classes that are similarly statistically distinguishable from each other.

We also examined absolute chr 15 *Krt* gene expression levels (Fig. 6, *A* and *B*), expressed as $\log_{10}$ values. As with chr 11 *Krt* and *Krtap* genes, expression of individual *class 3* genes remained relatively unchanged from *day 0* and throughout the postamputation period. However, the range of differences in the absolute expression of individual genes was quite broad and extended almost 170-fold in both strains, varying from the least expressed to the most highly expressed. *Class 2* genes cover a lower range of absolute expression levels, ~10-fold in both B6 and MRL strains at *day 0*. These genes start highly expressed at *day 0* in B6 but drop significantly at *day 3*. By contrast, in MRL the exact opposite is observed. Again, *class 2* genes possess similar expression levels at *day 7* and nearly identical expression levels at *day 14*.

The *class 1* genes, *Krt6a* and *Krt6b*, exhibit opposite expression behaviors in B6 vs. MRL to that of *class 2* genes; expression changed from *day 0* to *day 3* clearly opposite in B6, going from lower to higher expression level, compared with MRL, which started higher then decreased to a lower expression level. Expression levels at *days 3, 7,* and *14* were higher in B6 vs. MRL strains by a wide range from ~1.5-fold to 11-fold. These findings were confirmed by q-rtPCR.

Keratinocyte activation cycle: is uninjured MRL tissue in the activated state? Elevated expression levels of *Krt6*, *Krt16,* and *Krt17* are markers for an activated keratinocyte state, a state

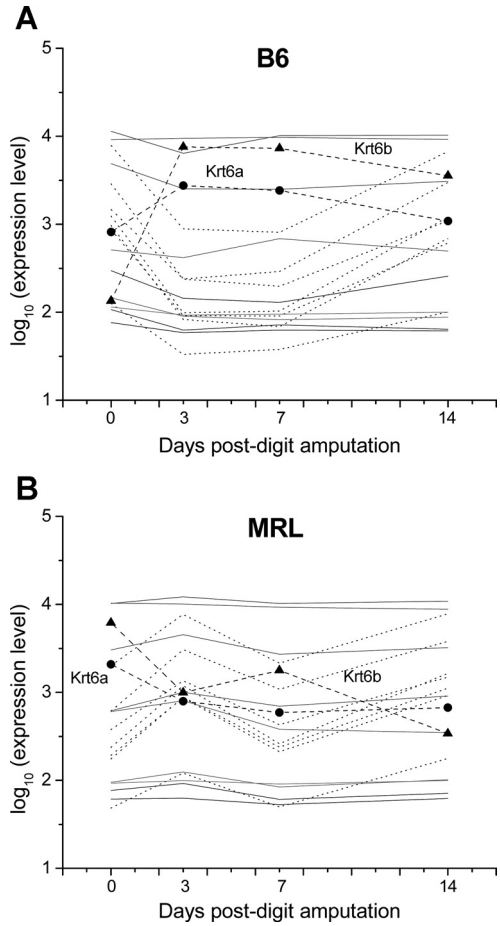

Fig. 6. Absolute temporal $\log_{10}$(expression Levels) of digit amputation RNAs for *Krts* and *Krtaps* located on Chromosome 15 in B6 (*A*) and in MRL (*B*). The 3 gene expression classes represented are described in the text. The 3 expression classes with line styles identified in Fig. 5 are used to code the individual lines in these plots.

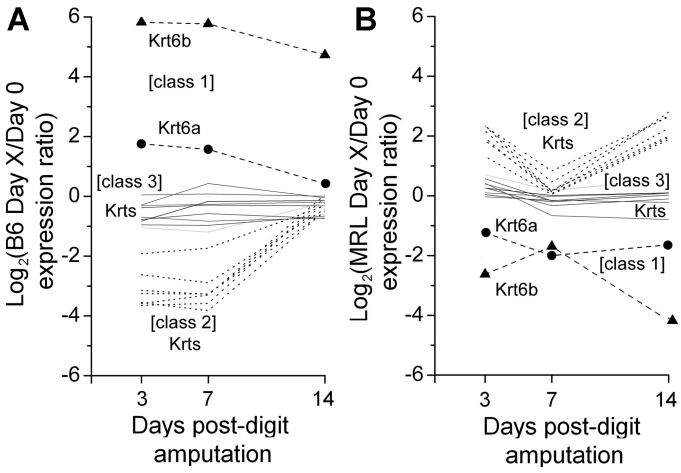

Fig. 5. Temporal $\log_2$(expression fold-change) of digit amputation RNAs for *Krts* and *Krtaps* located on Chromosome 15 are displayed for B6 in *A* and for MRL in *B*. The 3 gene expression classes represented are described in the text. Each line represents a single gene activity in B6 (*day 0* normalized values at *days 3, 7, 14*; *A*) and in MRL (*day 0* normalized values at *days 3, 7, 14*; *B*) strains. Three expression classes are indicated with different line styles to code the individual lines. Filled symbols indicate *Krt6a* and *Krt6b*.

associated with wound healing (30) and other pathological skin states such as psoriasis (44). Our data suggested that MRL mice may have keratinocytes in the activated state in uninjured tissue, while B6 mice do not. We tested this idea by examining the microarray expression levels of 40 genes known to be upregulated and associated with promoting and maintaining the keratinocyte activated state (17) and comparing their levels in MRL to B6 (Fig. 7, *A–D*). First, we examined all genes on the microarray chips for MRL and B6 in Fig. 7*A* (for *day 0*) and Fig. 7*B* (for *day 3*). For both days the great majority of these genes showed no differences in strain-specific expression fold-change, being clustered symmetrically about the slope = 1 line. However, there are thinly populated gene expression distributions that lie significantly above the +4 SD line as well as below the −4 SD line calculated from the total gene microarray data. Next, for MRL and B6 in Fig. 7*C* (*day 0*) and Fig. 7*D* (*day 3*) we examined just the 40 genes associated with the keratinocyte activated state. In Fig. 7*C*, eight of these biomarker genes had expression levels greater than the +4 SD line (same SD from Fig. 7*A* calculated from total microarray data); therefore, they are significantly greater in expression levels for MRL in unwounded tissue than for B6, suggesting that the MRL strain tissues exhibit the keratinocyte activated state. By postamputation *day 3* (Fig. 7*D*), seven of these same eight genes exhibit the opposite behavior, where their expression levels were below the −4 SD line (same SD as from Fig. 7*B*). Thus, at *day 3*, these B6 genes now display a keratinocyte activated state behavior, while MRL displays lower levels than at *day 0* and appears to exhibit gene activity consistent with a diminished level of keratinocyte activation. These data suggest that the MRL mice have at least some of their signaling networks tuned to exist in the activated state prior to wounding, whereas the B6 mice do not. Thus, MRL mice might gain a significant advantage over B6 mice in responding to an injury, including the potential to heal wounds more effectively and possibly scarlessly, as is the case with healing of MRL ear hole wounds (10).

Keratin gene and keratinocyte activation cycle association network analysis. We examined the keratinocyte activation state cycle model for MRL mice by performing a network-based analysis using Cytoscape and literature-based protein-protein linkages from String 8.2. The results are shown in Fig. 8 as a Cytoscape-generated image of the gene network connectivity integrated with the keratinocyte activation cycle model for *day 0* microarray expression ratios of the two strains. The network is based upon the keratinocyte activated state model presented in a recent review (17) and has the following features. Normal skin basal keratinocytes characteristically express Krt14 and Krt5, comprising an intermediate filament (IF) keratin pair in the mouse. Keratinocyte differentiation leads to preferential expression of the IF pair Krt10 and Krt1. The activated state expresses the IF pair Krt16 and Krt6, while the contractile state expresses Krt17. According to microarray expression data the Krt genes (gray diamonds in Fig. 8) show that the Krt16 and Krt6 genes are expressed at significantly higher levels in MRL compared with B6 at *day 0*, clearly indicating an activated state for MRL mice, but not B6 mice. Genes shown as white circles exhibited no significant differences between the two strains. Therefore, Krt17 (a contractile gene marker), Krt1, and Krt10 (a differentiation state IF pair), and Krt5 and Krt14 (a basal state IF pair) exhibit no expression difference in MRL mice vs. B6 mice at *day 0* (Fig. 8, Table 2).

Progression to the activated state is promoted by Il1, and that state is maintained by Tnf and Tgfa (17). We show that of three Il1 activation-promoting genes and receptors (Il1a, Il1b, Il1rn), only Il1b is more highly expressed in MRL mice, whereas the other two show no differences. The Tnf species is also differentially expressed, but to a lesser extent. The differentially expressed control genes Il1b and Tnf possess significant network connectivity to the keratinocyte activation state genes.

The genes presented within the box (dashed line in Fig. 8) are all genes that were reported to be upregulated in the keratinocyte activated state (17). On *day 0*, they are either more highly expressed in MRL vs. B6 strains or are not different at

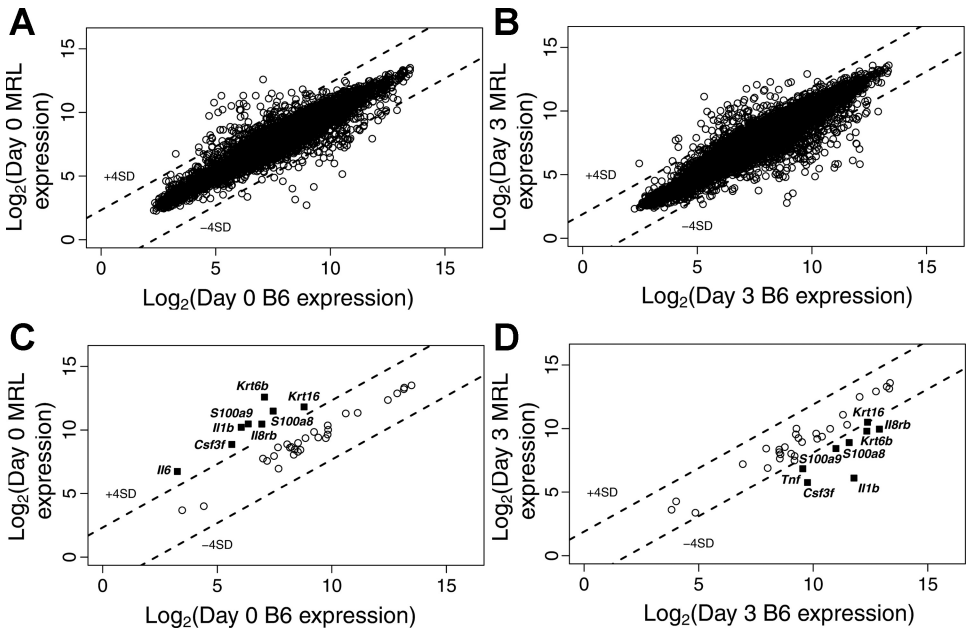

Fig. 7. Absolute $\log_2$(expression levels) for MRL vs. B6: for *day 0* (*A, C*) or *day 3* (*B, D*). In *A* and *B*, the entire microarray gene set values are presented for *day 0* and *day 3*, respectively. In *C* and *D*, the values for 40 selected genes involved in the keratinocyte activation cycle are presented for *day 0* and *day 3*, respectively. The identity of a subset of the genes is indicated whose values exhibit extreme differences in expression ratio between strains. In all panels, the + and −4 SD lines ($P < 0.000063$ criterion) are shown. These are calculated for the total gene distributions in *A* and *B*. The 4 SD lines in *A* and *C* are identical as are those in *B* and *D*. The identities are presented for 8 genes most different in expression level in *C* that fall outside the +4 SD line. Therefore, these 8 most different gene ratios are considered significantly different (better than $P < 0.000063$) from the entire microarray gene population. The same conclusion of high significance applies to the same identified genes exhibiting values below the −4 SD line in *D* (better than $P < 0.000063$).

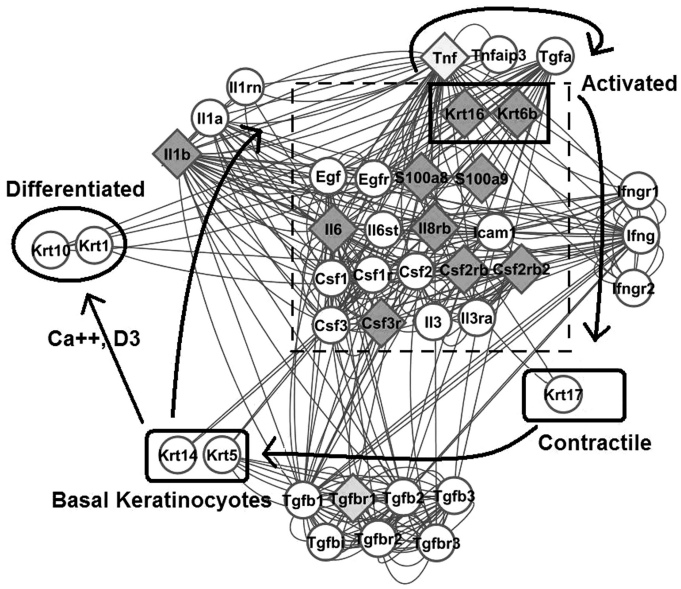

Fig. 8. A gene network expression view for *day 0* uninjured B6 and MRL strains tissues superimposed upon the keratinocyte activation cycle (17). The gene network view was created using STRING and Cytoscape as described in METHODS. The networks include the keratin genes involved in the different states of the cycle (within boxes or ovals), genes promoting transitions between states in the cycle (associated with cycle transition arrows), and those genes maintaining the activated state of the cycle and other genes known to be upregulated in the activated state (all inside the dashed box). Genes in diamond shapes are all >1.5-fold more highly expressed in MRL vs. B6 at *day 0* based upon their microarray data. Diamond symbols in light gray background are between 1.5- and 2.0-fold more highly expressed in MRL vs. B6 strains, while those in dark gray background are >2-fold more highly expressed. All other genes within white circle symbols exhibit no significant expression difference in MRL vs. B6 strains. The fngr1 and Tgfb2 genes exhibit slightly lower expression in MRL, but not enough to be colored gray.

all. The complete temporal gene expression data (Fig. 9) for six of the genes (*S100a8*, *S100a9*, *Il6*, *Csf3r*, *Il1b*, and *Tnf*) associated with *Krt6* and *Krt16* in the activated state show significantly higher expression levels in MRL compared with B6. At *day 3*, this relationship reverses for all six genes. By *day 7* through *day 14*, all six genes decline in expression, with higher expression levels maintained in B6. These gene expression behaviors are consistent with uninjured MRL tissue existing in a keratinocyte activated state, while the B6 tissue acquires the gene signatures of the keratinocyte activated state by *day 3* postinjury.

Immunohistochemical staining of keratin genes. Given the unusual expression behavior exhibited by the group of *class 1* genes *Krt16*, *Krt6a,* and *Krt6b* in B6 and MRL mice, we examined Krt16 protein expression via immunohistochemical (IHC) staining of *day 0* B6 and MRL uninjured digit tissue. As seen in Fig. 10, normal MRL and B6 digits showed expression of Krt16 protein in the epidermis as expected. Although B6 digit tissue (Fig. 10*A*) exhibited Krt16 staining of the surface keratinized layer, Krt16 was evident in the thickened multilayered epidermis in MRL (Fig. 10*B*), consistent with an activated keratinocyte phenotype in this uninjured tissue. These findings are consistent with our previous gene expression data demonstrating that uninjured MRL tissues exist in a keratin activated state rendering it more effective in responding to an injury.

Examination of injured digit tissue showed what appeared to be significant nonspecific staining, with binding to all structures, and therefore these studies have not been included. However, ear hole closure is representative of the regeneration process. Given that MRL mice have been previously shown to exhibit the complete regenerative process during ear hole closure (10), whereas digit healing in these mice is representative of incomplete regeneration that involves blastema formation, we examined Krt protein expression by IHC in MRL and B6 ear tissue during regeneration. In this case, we used ear tissue both pre- and postinjury from both strains. As a control keratin gene, we examined Krt10, a *class 3* gene that is not differentially expressed between MRL and B6 regenerating digits over time (see Fig. 4 and Table 2). Krt10, which is expressed in the epidermis of injured ear tissue, displays similar expression between MRL and B6 mice (Fig. 11, *A* and *B*, and Fig. 12 with quantitative data) and disappears from the injury site in both strains (arrows). This finding is consistent with our *Krt10* regenerating digit expression levels presented in Fig. 4 and Table 2. Krt6 and Krt16 proteins both show

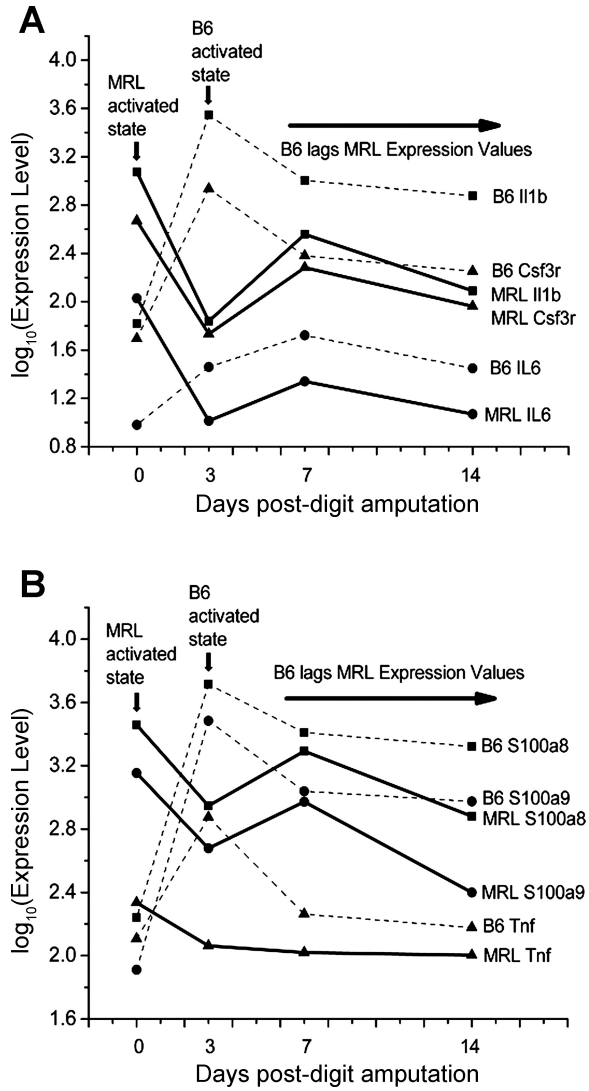

Fig. 9. Temporal $\log_{10}$ (expression Levels) of digit amputation RNAs for activation cycle genes. *A*: Il1b, Il6, and Csf3r genes in MRL and B6; *B*: S100a8, S100a9, and Tnf genes in MRL and B6 from microarray data. Genes for each strain are indicated for MRL (solid lines) and B6 (dashed lines) strains.

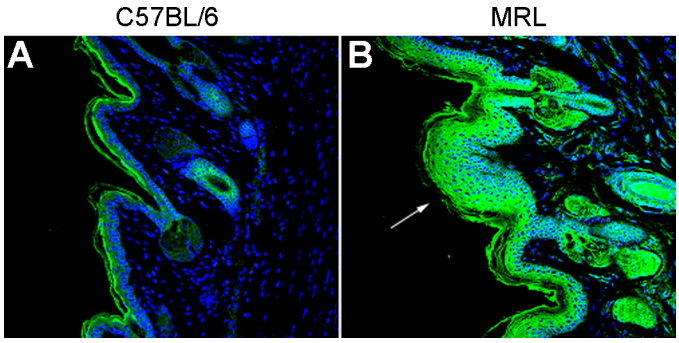

Fig. 10. Normal B6 (C57BL/6) and MRL digits stained for Krt16 proteins. B6 tissue (*A*) and MRL tissue (*B*) are stained with anti-Krt16 antibody (green). Nuclei were then counterstained with DAPI for DNA (blue). Arrow, activated keratinocyte phenotype.

epidermal expression in normal and injured ear tissue. Epidermal expression increases after injury in the regenerating MRL ear significantly more than in the B6 (Fig. 11, *C–F*, and Fig. 12). Following injury, populations of cells in the dermis now show expression of both Krt16 and Krt6 in the regenerating MRL tissue. Evidence for specific Krt6 and Krt16 MRL protein expression in the ear, but not Krt10 protein expression, supports the differential MRL vs. B6 strains' gene expression microarray data generated in the digit.

To determine the generality of the high expression levels of Krt16 in the MRL, we examined tissue from normal flank skin and small intestine. As seen in Fig. 13, our control Krt10 expression is similar between B6 and MRL in both tissues (low staining levels in MRL are nonspecific and noncell associated). However, staining of Krt16 and Krt6 (data not shown) is seen only in hair follicles in B6 but is found in the epidermis as well as the hair follicles in MRL. In the small intestine, no staining is seen in the B6, whereas epithelial and stromal cell staining is seen in the MRL. These results are consistent with the expression patterns seen in normal digit (Fig. 10) and normal ear pinna (Fig. 12), as well as the microarray results.

DISCUSSION

B6 and MRL mice show different healing properties after injury. Our analysis of gene expression after digit amputation has highlighted the different expression patterns of keratins in the MRL regenerative strain compared with the wound healing B6 strain. MRL and B6 digits possess similar temporal expres-

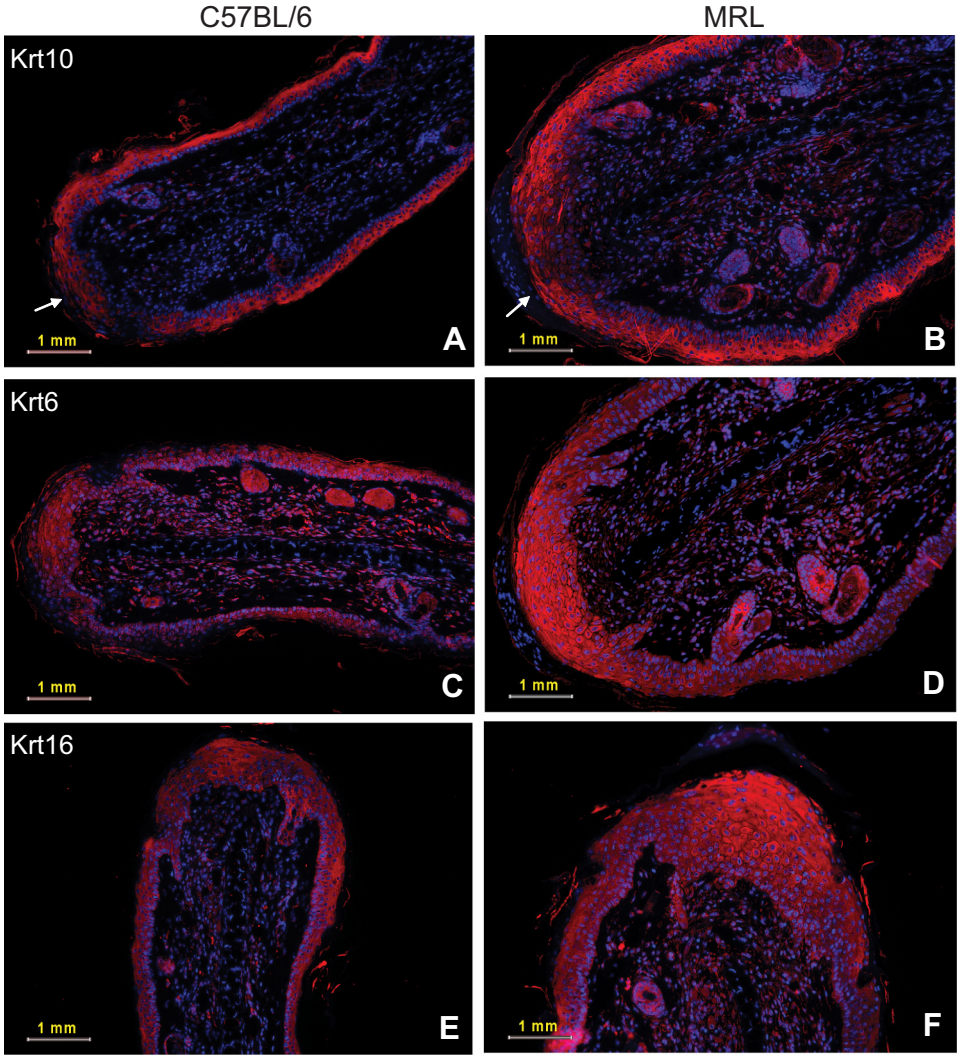

Fig. 11. Hole-punched (*day 7* postinjury) B6 (C57BL/6) (*A, C, E*) and MRL (*B, D, F*) ear tissue was stained with anti-Krt10 (*A, B*), anti-Krt 6 (*C, D*), and anti-Krt16 (*E, F*) primary and secondary (red) antibodies. Nuclei were then counterstained with DAPI (blue) for DNA. Immunofluorescent images are seen in this figure with labeling of epidermal injury sites indicated by arrows with size scale bars (1 mm) at the *left bottom* corner.

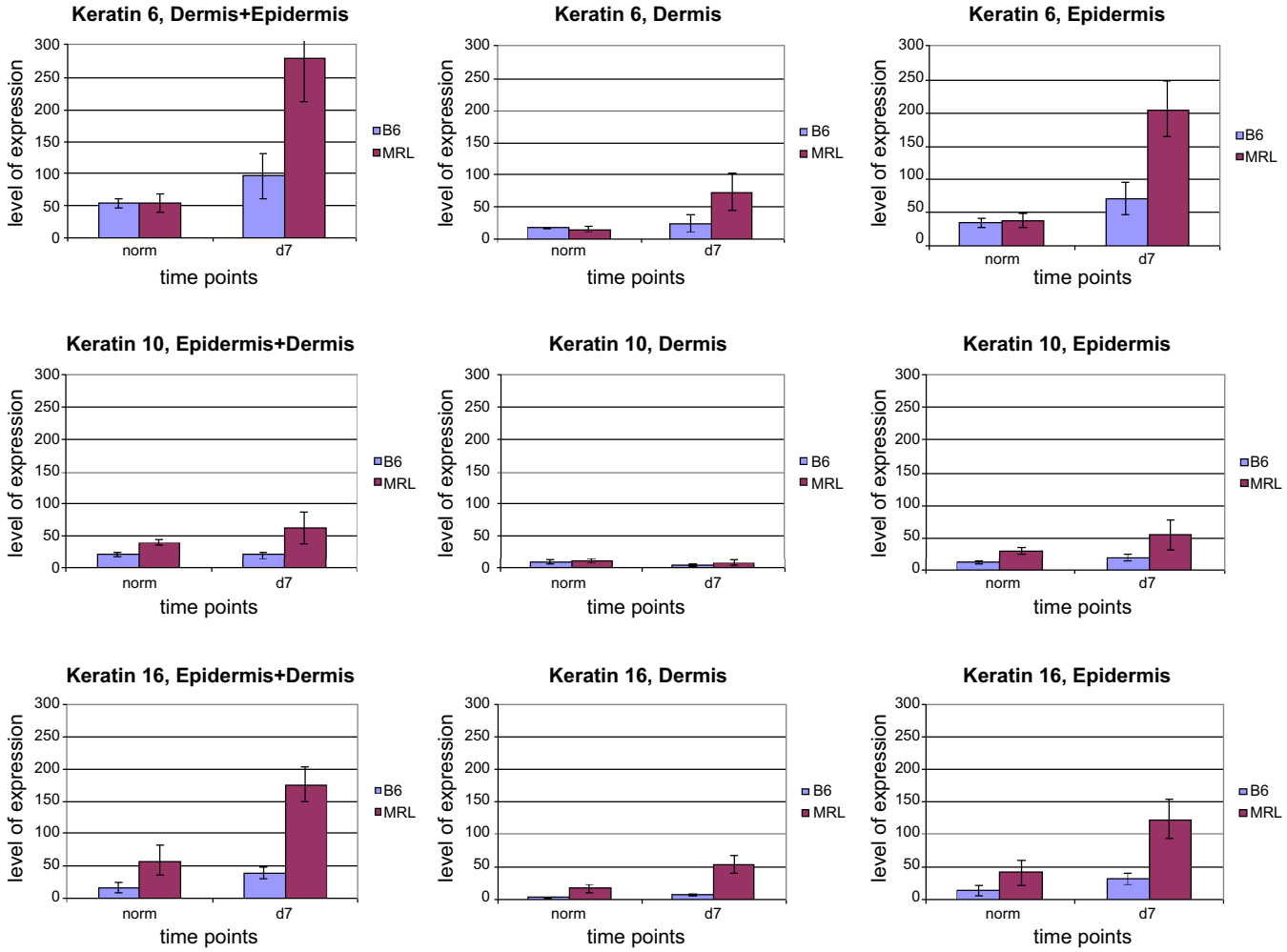

Fig. 12. Images from Fig. 11 and for *days 0* and *7* postinjury in MRL and B6 mouse ears were analyzed by ImageJv1.46f software provided by the NIH. The injury site was analyzed for total epidermal/dermal staining and epidermal staining separately. Then the value for epidermal staining was subtracted from the total staining value, providing the level of dermal staining. Standard error bars were derived from analysis of 3–4 images/strain/time point/keratin. Data are represented as means ± SE ($n = 3$).

sion levels in uninjured tissue for a group of genes, which we refer to as *class 3 Krt* and *Krtap* genes. We identified a second group, *class 2 Krt* and *Krtap* genes, which have different starting expression levels, with B6 being greater than MRL. At *day 3*, expression levels in *class 2* genes change, with B6 levels uniformly dropping while MRL levels uniformly increase. The opposite temporal behavior is true for only two *Krt* genes that comprise *class 1* gene responses: *Krt6a* and *Krt6b* on chromosome 15 and *Krt16* on chromosome 11. These behaviors suggest that the switch in expression levels for both *class 2* and *class 1* genes between *day 0* and *3* for these two strains is critical for the differential biological response noted previously in their response to wounding events. In particular, unique Krt6 and Krt16 responses correlate with immunohistochemical evidence from tissue sections from normal digit and interestingly correlate with the rapid scarless healing of ear hole injury sites in MRL, but not B6 (10, 20).

In healthy epidermis, basal keratinocytes are considered to be in the inactivate state and proliferate slowly in the basal layer but differentiate in the suprabasal layer. During wounding or in pathological states involving injury to tissue, basal keratinocytes are induced to the activated state whose characteristics include migration, hyperproliferation, secretion of signaling molecules and extracellular matrix components, as well as alterations in specific keratin production. In particular, Krt6, Krt16, and Krt17 have been demonstrated to be markers of this activated state in the mouse, and a keratinocyte activation cycle has been proposed (17). Progression through this activation cycle has been proposed to be under the control of signaling proteins, with the conversion from basal keratinocyte to activated keratinocyte initiated by IL-1. TNF-α is subsequently induced, and this maintains the activated state of the keratinocyte through an autocrine feedback mechanism. In turn, a host of other factors are activated, including S100a8, S100a9, TGF-α, IL-1a, IL receptor agonist, IL-3, IL-6, IL-8, Egf, Egfr, Icam-1, Csf1, Csf2, and Csf3.

One reason for the Krt6/Krt16 pair upregulation in the activated state is that these two gene products interact, forming a specific type of keratin IF within keratinocytes. Keratin IFs serve different purposes but occur predominantly in keratin gene pairs comprising one each of a type I and type II keratin. These interacting keratin proteins tend to be expressed in pairs

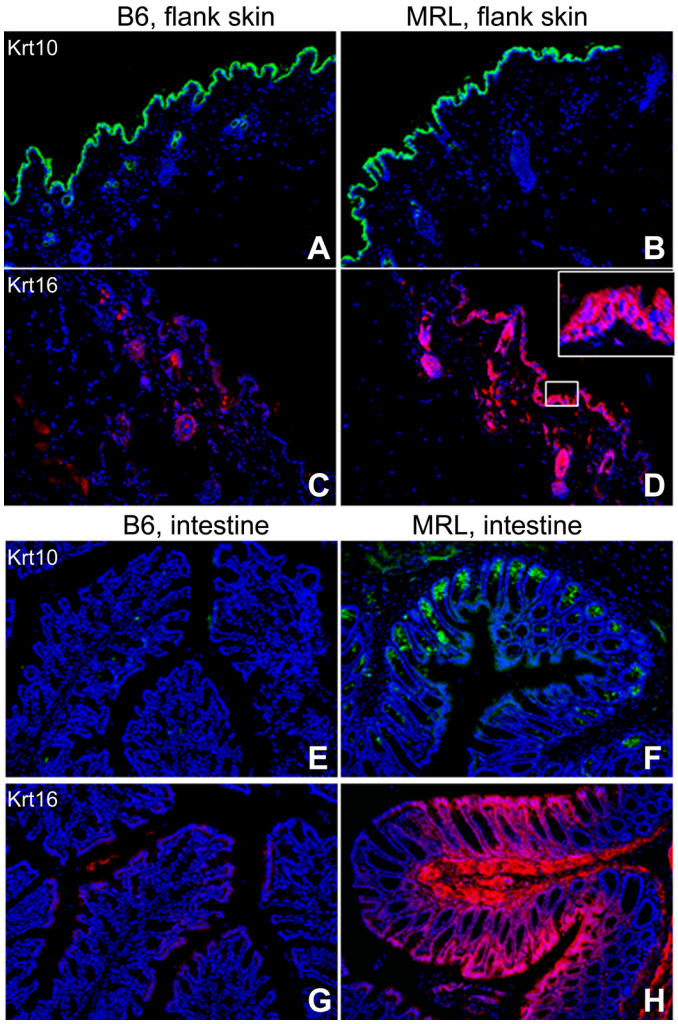

Fig. 13. Normal B6 (C57BL/6) and MRL flank skin and small intestine stained for Krt10 and Krt16 proteins. In *A, B, E,* and *F*, B6 tissue and MRL tissue are stained with anti-Krt10 antibody (green). In *C, D, G,* and *H*, tissue is stained with anti-Krt16 antibody (red). Nuclei were then counterstained with DAPI for DNA (blue).

as the specific keratin IF is needed. It is believed that the Krt6/Krt16 pair form a necessary keratin IF for the activated keratinocyte to respond to the injury, as a study of the loss of the *Krt6* gene reveals (46). Signals from IFN-γ induce Krt17 expression that results in keratinocytes becoming contractile; this promotes shrinking of the provisional basement membrane. Finally, fibroblast-secreted TGF-β signals induce Krt5 and Krt14 expression that converts the activated keratinocytes back to the basal state, thereby completing the activation cycle as the tissue has healed (17).

It is known from other expression studies that Krt6 is coexpressed with Krt16 under certain circumstances, such as following wounding (16, 29, 38), in psoriasis (19), and in graft-vs.-host disease (36). Our results confirm that, like *Krt16* on chromosome 11, *Krt6* on chromosome 15 shows similar expression patterns for B6 vs. MRL mice that are exactly the opposite of all other *Krt* and *Krtap* expression patterns. In particular, at *day 0,* prior to wounding, the *Krt6* and *Krt16* genes are highly expressed in MRL, but not B6 strains, suggesting the occurrence of the keratinocyte activated state in MRL, but not in B6. This was corroborated at the protein level by our IHC results showing that in uninjured digit tissue the MRL digit had significantly greater Krt16 staining throughout a multilayered epidermal region, compared with a thin epidermal region for B6.

The upregulation of a number of important genes other than keratins also supports this keratinocyte activation state existing in the uninjured MRL tissue. The IL-1 signaling gene is considered the gene responsible for converting from the basal keratinocyte state, found in normal mouse skin, to the activated keratinocyte state observed following wounding and other pathological conditions (17). We observed the Il1b gene product to be significantly expressed in MRL mice at *day 0*, but not in B6. The S100a8 and S100a9 gene products are also associated at elevated expression levels in the activated state, having been observed elevated along with Krt6 and Krt16, perhaps interacting with them as a heterodimeric protein. Most of these species have been observed during wound healing (38), psoriasis (45), graft-vs.-host disease (36), and in human pterygium, an ocular surface disease characterized by aberrant wound healing (41). Conversely, Krt16 is reduced in chronic wounds where re-epithelialization is not occurring (35). The *S100a8* and *S100a9* genes are Ca^{2+}-dependent cell cycle control genes and may be involved in the inflammatory response. Interestingly, in a wound healing study of the PU.I null mouse, the "macrophageless" mouse, which lacks a standard inflammatory response and heals with reduced fibrosis, the *Krt6*, *S100a8,* and *S100a9* genes were all upregulated, although *IL-6*, which is normally upregulated in wounds, was absent from null mouse wound sites (12). In a study of mouse skin wounds versus oral mucosal wounds, *IL-1a*, *IL-1b,* and *TNF-α* were not overexpressed in mucosal wounds but were in skin wounds in which was seen a lowered inflammatory response and scarring (8). In this study *IL-1b* stimulation of keratinocytes produced an elevated *IL-6* response in skin keratinocytes but not mucosal keratinocytes. These studies indicate that differences in inflammatory responses of tissues undergoing repair are important in determining differences in these key gene expression levels due to the existence of critical pathway differences. Upregulation of these key genes in uninjured MRL but not B6 digit tissue is correlated with faster healing and less scarring in the MRL compared with B6, and it suggests that strain differences in inflammatory responses may exist as well. The positive effect of the inflammatory response during regeneration has been noted previously (15, 24).

There is evidence that S100a8 and S100a9 associate physically with the keratin IF formed by Krt6 and Krt16, perhaps as a heterodimeric protein. Clearly, network connectivity is exhibited in Fig. 8 between *Krt6* and *Krt16* and the *S100a8* and *S100a9* genes, suggestive of a potential physical association since Cytoscape database linkages are based in part upon physical interactions reported in the literature. Both *S100a8* and *S100a9* genes are significantly overexpressed in MRL vs. B6 mouse tissues, to nearly the same extent as are *Krt6* and *Krt16*, supporting the idea of a keratinocyte activation-like state for normal MRL tissue. Finally, the temporal expression of *Krt6*, *Krt16*, *S100a8*, *S100a9*, *Csf3*, *Tnf, IL-6,* and *IL-1b* all were shown to peak 3 days later in B6 compared with MRL, following which they decline slowly to *day 14* in both strains, but always remaining higher in expression level in B6 compared with MRL. This is exactly the behavior to be expected if

MRL uninjured tissue exists in the keratinocyte activated state, while B6 reaches that state a few days following injury, always lagging temporally behind the MRL in the Keratinocyte Activation Cycle.

While we noted the major keratinocyte activation state genes that are highly expressed at *day 0* in MRL, but not in B6, a number of genes in this class are not expressed differently between the two strains. These genes suggest alternate explanations for this phenomenon. It could be that only a fraction of the cells from which the RNA was isolated are activation state keratinocytes, which can confound the expression ratio interpretation. Another explanation is that an incomplete activation state or an activation state-like behavior of the genes is being expressed because not all of the signaling networks characterizing the activated state are activated. Nonetheless, the MRL strain might gain a significant advantage over B6 in more effectively dealing with any impending injury situation by existing in this activated state preinjury. The tissue is predisposed to respond to the injury situation and can then recover more quickly, heal without scarring, and close ear hole wounds in MRL (10, 20).

Examination of Krt16 protein expression using IHC in uninjured digit tissues of MRL and B6 showed different expression patterns. In uninjured B6 digit tissue, Krt16 was not expressed in epidermal cells but in the keratinized surface layer of the tissue. On the other hand, in uninjured MRL tissue, Krt16 was expressed in what appears to be a hyperproliferative epidermis. This is completely consistent with what is described from our gene expression studies as a keratinocyte activated state only in uninjured MRL tissue.

Though we did not show microarray gene expression data from ear tissue, examination of MRL and B6 injured ear sections shows protein expression that is consistent with the *Krt* digit expression patterns in the two strains. Thus, for *class 3* Krt proteins, Krt10 showed no differences between MRL and B6. For *class 1* Krt proteins, Krt6 and Krt16 showed higher protein expression in MRL epidermis immediately after injury. Since MRL ear holes regenerate completely (10), and MRL digits only show incomplete regeneration (20), it may be that the downregulation of *Krt6 and Krt16* expression in the MRL digit by *day 3* following injury may be responsible for incomplete regeneration of the digit. Krt16 showed unique activity in the dermis of the MRL ear postinjury. This is especially interesting because previous studies in regenerating newt limb show that keratins were expressed in the dermal tissue and specifically in the regenerating blastema (13, 16). Furthermore, from various genetic mapping studies of MRL and LG/J ear hole closure, a narrowed genetic locus on chr 11 containing *Krt* genes has been identified and *Krt16* is a candidate gene (2, 3, 9, 23). This would indicate a genetic difference in *Krt16* due to polymorphisms found in noncoding regions, leading to differences in regulation of gene expression. Finally, enhanced keratinocyte activity in the MRL mouse during ear hole closure (10) and digit injury (20) has been seen in that re-epithelialization occurs within 48 h in the ear and before 1 wk in the digit, whereas this will occur in the B6 over a 1 to 2 wk period. Rapid re-epithelialization occurring within 24 h after injury is an important property of amphibian regeneration (28, 34, 39).

That Krt16 protein is highly expressed in normal MRL flank skin epidermis is at odds with the findings that MRL dorsal skin does not heal differently or possibly more poorly than B6 skin (1, 14), though we do not have expression data on postinjury skin. On the other hand, it supports the data showing that a skin graft placed in an MRL skin wound heals much better than the control strain and without scar formation (40), suggesting that something other than keratinocyte activation and proliferation is responsible. The striking Krt16 expression in the MRL small intestine may indicate a highly regenerative organ, especially with the high level of expression in the nonepithelial stroma, which may be similar to that seen in the regenerating MRL ear.

GRANTS

These studies were supported by DOD/DARPA Grant W911NF-06-1-0067 (K. A. Marx). We also acknowledge support from NIH (E. Heber-Katz), Grants HL-080948 (C. J. Hatcher), R01 HL-61785 (C. T. Basson, C. J. Hatcher), RC1 HL-100579 (C. T. Basson, C. J. Hatcher), and the Snart Cardiovascular Fund (C. J. Hatcher, C. T. Basson).

DISCLOSURES

No conflicts of interest, financial or otherwise, are declared by the author(s).

AUTHOR CONTRIBUTIONS

Author contributions: C.-H.C., J.L., C.J.H., C.T.B., E.H.-K., and K.A.M. conception and design of research; C.-H.C., J.L., X.-M.Z., K.B., D.G., C.J.H., and K.A.M. performed experiments; C.-H.C., D.G., C.J.H., C.T.B., E.H.-K., and K.A.M. analyzed data; C.-H.C., C.J.H., C.T.B., E.H.-K., and K.A.M. interpreted results of experiments; C.-H.C., D.G., C.J.H., and E.H.-K. prepared figures; C.-H.C., C.J.H., C.T.B., E.H.-K., and K.A.M. drafted manuscript; C.-H.C., C.J.H., C.T.B., E.H.-K., and K.A.M. edited and revised manuscript; C.-H.C., J.L., X.-M.Z., K.B., D.G., C.J.H., C.T.B., E.H.-K., and K.A.M. approved final version of manuscript.

REFERENCES

1. **Beare AHM, Metcalfe AD, Ferguson MWJ.** Location of injury influences the mechanisms of both regeneration and repair within the MRL/MpJ mouse. *J Anat* 209: 547–559, 2006.
2. **Blankenhorn EP, Bryan G, Kossenkov AV, Clark LD, Zhang XM, Chang C, Horng W, Pletscher LS, Cheverud JM, Showe LC, Heber-Katz E.** Genetic loci that regulate healing and regeneration in LG/J and SM/J mice. *Mamm Genome* 20: 720–733, 2009.
3. **Blankenhorn EP, Troutman S, Clark LD, Zhang XM, Chen P, Heber-Katz E.** Sexually dimorphic genes regulate healing and regeneration in MRL mice. *Mamm Genome* 14: 250–260, 2003.
4. **Borgens RB.** Mice regrow the tips of their foretoes. *Science* 217: 747–750, 1982.
5. **Breitling R.** Biological microarray interpretation: the rules of engagement. *Biochim Biophys Acta* 1759: 319–327, 2006.
6. **Brockes JP, Kumar A.** Appendage regeneration in adult vertebrates and implications for regenerative medicine. *Science* 310: 1919–1923, 2005.
7. **Chadwick RB, Bu L, Yu H, Hu Y, Wergedal JE, Mohan S, Baylink DJ.** Digit tip regrowth and differential gene expression in MRL/Mpj, DBA/2, and C57BL/6 mice. *Wound Repair Regen* 15: 275–284, 2007.
8. **Chen L, Arbieva ZH, Guo S, Marucha PT, Mustoe TA, DiPietro LA.** Positional differences in the wound transcriptome of skin and oral mucosa. *BMC Genomics* 11: 471, 2010.
9. **Cheverud JM, Lawson HA, Funk R, Zhou J, Blankenhorn EP, Heber-Katz E.** Healing quantitative trait loci in a combined cross analysis using related mouse strain crosses. *Heredity* 108: 441–446, 2012.
10. **Clark LD, Clark RK, Heber-Katz E.** A new murine model for mammalian wound repair and regeneration. *Clin Immunol Immunopathol* 88: 35–45, 1998.
11. **Cline MS, Smoot M, Cerami E, Kuchinsky A, Landys N, Workman C, Christmas R, Avila-Campilo I, Creech M, Gross B, Hanspers K, Isserlin R, Kelley R, Killcoyne S, Lotia S, Maere S, Morris J, Ono K, Pavlovic V, Pico AR, Vailaya A, Wang PL, Adler A, Conklin BR, Hood L, Kuiper M, Sander C, Schmulevich I, Schwikowski B, Warner GJ, Ideker T, Bader GD.** Integration of biological networks and gene expression data using Cytoscape. *Nat Protoc* 2: 2366–2382, 2007.
12. **Cooper L, Johnson C, Burslem F, Martin P.** Wound healing and inflammation genes revealed by array analysis of 'macrophageless' PU.1 null mice. *Genome Biol* 6: R5, 2004.

13. **Corcoran JP, Ferretti P.** Keratin 8 and 18 expression in mesenchymal progenitor cells of regenerating limbs is associated with cell proliferation and differentiation. *Dev Dyn* 210: 355–370, 1997.
14. **Davis TA, Amare M, Naik S, Kovalchuk AL, Tadaki D.** Differential cutaneous wound healing in thermally injured MRL/MPJ mice. *Wound Repair Regen* 15: 577–588, 2007.
15. **De Franco M, Carneiro Pdos S, Peters LC, Vorraro F, Borrego A, Ribeiro OG, Starobinas N, Cabrera WK, Ibañez OM.** Slc11a1 (Nramp1) alleles interact with acute inflammation loci to modulate wound-healing traits in mice. *Mamm Genome* 18: 263–269, 2007.
16. **Ferretti P, Brockes JP, Brown R.** A newt type II keratin restricted to normal and regenerating limbs and tails is responsive to retinoic acid. *Development* 111: 497–507, 1991.
17. **Freedberg IM, Tomic-Canic M, Komine M, Blumenberg M.** Keratins and the keratinocyte activation cycle. *J Invest Dermatol* 116: 633–640, 2001.
18. **Goss RJ, Grimes LN.** Epidermal downgrowths in regenerating rabbit ear holes. *J Morphol* 146: 533–542, 1975.
19. **Gottlieb AB, Krueger JG, Wittkowski K, Dedrick R, Walicke PA, Garovoy M.** Psoriasis as a model for T-cell-mediated disease: immunobiologic and clinical effects of treatment with multiple doses of efalizumab, an anti-CD11a antibody. *Arch Dermatol* 138: 591–600, 2002.
20. **Gourevitch DL, Clark L, Bedelbaeva K, Leferovich J, Heber-Katz E.** Dynamic changes after murine digit amputation: the MRL mouse digit shows waves of tissue remodeling, growth, and apoptosis. *Wound Repair Regen* 17: 447–455, 2009.
21. **Han M, Yang X, Taylor G, Burdsal CA, Anderson RA, Muneoka K.** Limb regeneration in higher vertebrates: developing a roadmap. *Anat Rec B New Anat* 287: 14–24, 2005.
22. **Hatcher CJ, Diman NY, Kim MS, Pennisi D, Song Y, Goldstein MM, Mikawa T, Basson CT.** A role for Tbx5 in proepicardial cell migration during cardiogenesis. *Physiol Genomics* 18: 129–140, 2004.
23. **Heber-Katz E, Chen P, Clark L, Zhang XM, Troutman S, Blankenhorn EP.** Regeneration in MRL mice: further genetic loci controlling the ear hole closure trait using MRL and M.m. Castaneus mice. *Wound Repair Regen* 12: 384–392, 2004.
24. **Heber-Katz E, Gourevitch D.** The relationship between inflammation and regeneration in the MRL mouse: potential relevance for putative human regenerative (scarless wound healing) capacities? *Ann NY Acad Sci* 1172: 110–114, 2009.
25. **Illingworth CM.** Trapped fingers and amputated finger tips in children. *J Pediatr Surg* 9: 853–858, 1974.
26. **Jensen LJ, Kuhn M, Stark M, Chaffron S, Creevey C, Muller J, Doerks T, Julien P, Roth A, Simonovic M, Bork P, von Mering C.** STRING 8–a global view on proteins and their functional interactions in 630 organisms. *Nucleic Acids Res* 37: D412–D416, 2009.
27. **Kench JA, Russell DM, Fadok VA, Young SK, Worthen GS, Jones-Carson J, Henson JE, Henson PM, Nemazee D.** Aberrant wound healing and TGF-beta production in the autoimmune-prone MRL/+ mouse. *Clin Immunol* 92: 300–310, 1999.
28. **Lash JW.** Studies on wound closure in urodeles. *J Exp Zool* 128: 13–28, 1995.
29. **Mansbridge JN, Knapp AM.** Changes in keratinocyte maturation during wound healing. *J Invest Dermatol* 89: 253–263, 1987.
30. **Mazzalupo S, Wong P, Martin P, Coulombe PA.** Role for keratins 6 and 17 during wound closure in embryonic mouse skin. *Dev Dyn* 226: 356–365, 2003.
31. **Singer M, Weckesser EC, Geraudie J, Maier CE, Singer J.** Open finger tip healing and replacement after distal amputation in rhesus monkey with comparison to limb regeneration in lower vertebrates. *Anat Embryol (Berl)* 177: 29–36, 1987.
32. **Soderberg T, Nystrom A, Hallmans G, Hulten J.** Treatment of fingertip amputations with bone exposure. A comparative study between surgical and conservative treatment methods. *Scand J Plast Reconstr Surg* 17: 147–152, 1983.
33. **Stocum DL.** Amphibian regeneration and stem cells. *Curr Top Microbiol Immunol* 280: 1–70, 2004.
34. **Stocum DL.** Stages of forelimb regeneration in Ambystoma maculatum. *J Exp Zool* 209: 395–416, 1979.
35. **Stojadinovic O, Brem H, Vouthounis C, Lee B, Fallon J, Stallcup M, Merchant A, Galiano RD, Tomic-Canic M.** Molecular pathogenesis of chronic wounds: the role of beta-catenin and c-myc in the inhibition of epithelialization and wound healing. *Am J Pathol* 167: 59–69, 2005.
36. **Sugerman PB, Faber SB, Willis LM, Petrovic A, Murphy GF, Pappo J, Silberstein D, van den Brink MR.** Kinetics of gene expression in murine cutaneous graft-versus-host disease. *Am J Pathol* 164: 2189–2202, 2004.
37. **Tarca AL, Romero R, Draghici S.** Analysis of microarray experiments of gene expression profiling. *Am J Obstet Gynecol* 195: 373–388, 2006.
38. **Thorey IS, Roth J, Regenbogen J, Halle JP, Bittner M, Vogl T, Kaesler S, Bugnon P, Reitmaier B, Durka S, Graf A, Wöckner M, Rieger N, Konstantinow A, Wolf E, Goppelt A, Werner S.** The Ca^{2+}-binding proteins S100A8 and S100A9 are encoded by novel injury-regulated genes. *J Biol Chem* 276: 35818–35825, 2001.
39. **Thornton CS.** Amphibian limb regeneration. *Adv Morphog* 7: 205–249, 1968.
40. **Tolba RH, Schildberg FA, Decker D, Abdullah Z, Büttner R, Minor T, Von Ruecker A.** Mechanisms of improved wound healing in Murphy Roths Large (MRL) mice after skin transplantation. *Wound Repair Regen* 18: 662–670, 2010.
41. **Tong L, Chew J, Yang H, Ang LP, Tan DT, Beuerman RW.** Distinct gene subsets in pterygia formation and recurrence: dissecting complex biological phenomenon using genome wide expression data. *BMC Med Genomics* 2: 14, 2009.
42. **Tusher VG, Tibshirani R, Chu G.** Significance analysis of microarrays applied to the ionizing radiation response. *Proc Natl Acad Sci USA* 98: 5116–5121, 2001.
43. **Vidal P, Dickson MG.** Regeneration of the distal phalanx. A case report. *J Hand Surg Br* 18:230–233, 1993.
44. **Wojcik SM, Longley MA, Roop DR.** Discovery of a novel murine keratin 6 (K6) isoform explains the absence of hair and nail defects in mice deficient for K6a and K6b. *J Cell Biol* 154: 619–630, 2001.
45. **Wolk K, Witte E, Wallace E, Döcke WD, Kunz S, Asadullah K, Volk HD, Sterry W, Sabat R.** IL-22 regulates the expression of genes responsible for antimicrobial defense, cellular differentiation, and mobility in keratinocytes: a potential role in psoriasis. *Eur J Immunol* 36: 1309–1323, 2006.
46. **Wong P, Coulombe PA.** Loss of keratin 6 (K6) proteins reveals a function for intermediate filaments during wound repair. *J Cell Biol* 163: 327–337, 2003.
47. **Zhao W, Neufeld DA.** Bone regrowth in young mice stimulated by nail organ. *J Exp Zool* 271: 155–159, 1995.